Near-coastal circulation in the Northern Humboldt Current System from shipboard ADCP data

Alexis Chaigneau, Noel Dominguez, Gérard Eldin, Roberto Flores, Carmen Grados, Vincent Echevin

JOURNAL OF GEOPHYSICAL RESEARCH: OCEANS, VOL. 118, 5251–5266, doi:10.1002/jgrc.20328, 2013

Near-coastal circulation in the Northern Humboldt Current System from shipboard ADCP data

Alexis Chaigneau,[1,2] Noel Dominguez,[3] Gérard Eldin,[1,2] Luis Vasquez,[3] Roberto Flores,[3] Carmen Grados,[3] and Vincent Echevin[1,4]

Received 20 December 2012; revised 25 July 2013; accepted 25 July 2013; published 15 October 2013.

[1] The near-coastal circulation of the Northern Humboldt Current System is described analyzing ~8700 velocity profiles acquired by a shipboard acoustic Doppler current profiler (SADCP) during 21 surveys realized between 2008 and 2012 along the Peruvian coast. This data set permits observation of (i) part of the Peru Coastal Current and the Peru Oceanic Current that flow equatorward in near-surface layers close to the coast and farther than ~150 km from the coast, respectively; (ii) the Peru-Chile Undercurrent (PCUC) flowing poleward in subsurface layers along the outer continental shelf and inner slope; (iii) the near-surfacing Equatorial Undercurrent renamed as Ecuador-Peru Coastal Current that feeds the PCUC; and (iv) a deep equatorward current, referred to as the Chile-Peru Deep Coastal Current, flowing below the PCUC. A focus in the PCUC core layer shows that this current exhibits typical velocities of 5–10 cm s^{-1}. The PCUC deepens with an increasing thickness poleward, consistent with the alongshore conservation of potential vorticity. The PCUC mass transport increases from ~1.8 Sv at 5°S to a maximum value of ~5.2 Sv at 15°S, partly explained by the Sverdrup balance. The PCUC experiences relatively weak seasonal variability and the confluence of eddy-like structures and coastal currents strongly complicates the circulation. The PCUC intensity is also affected by the southward propagation of coastally trapped waves, as revealed by a strong PCUC intensification in March 2010 coincident with the passage of a downwelling coastal wave associated with a weak El Niño event.

Citation: Chaigneau, A., N. Dominguez, G. Eldin, L. Vasquez, R. Flores, C. Grados, and V. Echevin (2013), Near-coastal circulation in the Northern Humboldt Current System from shipboard ADCP data, *J. Geophys. Res. Oceans*, *118*, 5251–5266, doi:10.1002/jgrc.20328.

1. Introduction

[2] In the Northern part of the Humboldt Current system (NHCS), the ocean circulation is mostly wind-driven by the South Pacific subtropical anticyclone forcing the South Pacific gyre (Figure 1) whose eastern flank comprises the equatorward Peru Oceanic Current (POC). In the offshore ocean off the Ecuadorian and Peruvian coasts, this current feeds the South Equatorial Current (SEC) that flows westward in the near-surface layers (Figure 1a) [*Strub et al*., 1998; *Kessler*, 2006]. The SEC is forced by the permanent easterlies that pile up surface water toward the western equatorial Pacific creating a zonal eastward pressure gradient force that drives, in subsurface layers, the eastward flowing Equatorial Undercurrent (EUC) centered along the equator (Figure 1b) [e.g., *Philander*, 1973] and reaching the Galapagos Islands near 90°W. East of the archipelago, the EUC separates into two branches, one branch flowing southeastward to reach the Peruvian coast at ~5°S, while the other branch remains trapped along the equator [*Lukas*, 1986; *Kessler*, 2006; *Karnauskas et al*., 2010; *Collins et al*., 2013]. Below the thermocline and further South are found the primary and secondary Southern Subsurface Countercurrents (SSCCs), also referred to as Tsuchiya jets, that flow eastward and enter the NHCS along nominal latitudes of ~5°S and ~7°S, respectively [*Johnson and Moore*, 1997; *Rowe et al*., 2000; *Montes et al*., 2010, 2011; *Stramma et al*., 2010; *Czeschel et al*., 2011]. Near the Peruvian coast, the dominant alongshore equatorward winds and cyclonic wind-stress curl lead to an intense upwelling characterized by an alongshore narrow strip of cold (Figure 1b, color shading) and highly productive water and a current system composed of equatorward surface and mainly poleward subsurface flows. The equatorward surface circulation is composed of the Peru Coastal Current (PCC) that is mainly wind-driven [e.g., *Wyrtki*, 1966, 1967], but also reinforced, through geostrophic adjustment, by the

[1]Institut de Recherche pour le Développement, Toulouse, France.
[2]Laboratoire d'Études en Géophysique et Océanographie Spatiale, UMR CNRS, CNES, IRD, Université P. Sabatier, Toulouse, France.
[3]Instituto del MAR de PErú, Callao, Perú.
[4]Laboratoire d'Océanographie et de Climatologie: Expérimentation et Analyse Numérique, UMR CNRS, IRD/MNHN, Université Pierre et Marie Curie, Paris, France.

Corresponding author: A. Chaigneau, Laboratoire d'Études en Géophysique et Océanographie Spatiale, 14. Av. Edouard Belin, Toulouse FR-31400, France. (alexis.chaigneau@ird.fr)

2169-9275/13/10.1002/jgrc.20328

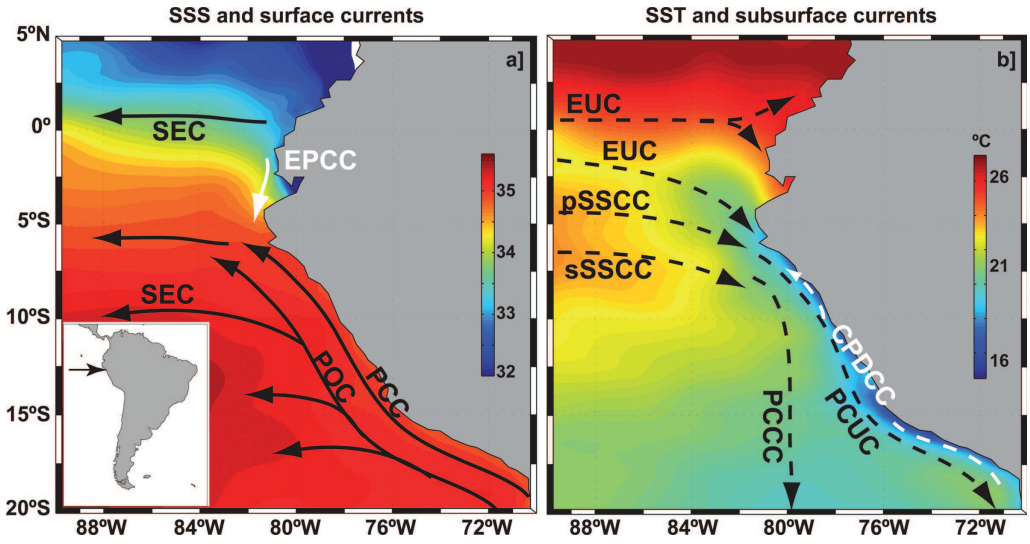

Figure 1. Sea surface properties and oceanic circulation scheme. (a) Sea-surface salinity (SSS, color shading) and surface circulation. (b) Sea-surface temperature (SST, color shading in °C) and subsurface circulation. SST and SSS were derived from the CARS 2009 climatology [*Ridgway et al*., 2002]. This figure was adapted from *Penven et al*. [2005], *Kessler* [2006], *Montes et al*. [2010], *Czeschel et al*. [2011], and *Mollier-Vogel et al*. [2012]. The newly defined Ecuador-Peru Coastal Current (EPCC) and Chile-Peru Deep Coastal Current (CPDCC) are indicated by white arrows. Surface currents. SEC: South Equatorial Current; EPCC: Ecuador-Peru Coastal Current; POC: Peru Oceanic Current; PCC: Peru Coastal Current. Subsurface currents. EUC: Equatorial Undercurrent; pSSCC: primary (northern branch) Southern Subsurface Countercurrent; sSSCC: secondary (southern branch) Southern Subsurface Countercurrent; PCCC: Peru-Chile Countercurrent; PCUC: Peru-Chile Undercurrent; CPDCC: Chile-Peru Deep Coastal Current.

cross-frontal temperature (and density) gradient due to the upwelling (Figure 1b, color shading). The subsurface poleward circulation is mainly composed of the Peru-Chile Undercurrent (PCUC) along the Peruvian continental shelf and slope (Figure 1b) and a weaker secondary poleward flow, the Peru-Chile Countercurrent (PCCC), that flows almost due south along ~80°–85°W (Figure 1b) [*Wyrtki*, 1963; *Huyer et al*., 1991; *Penven et al*., 2005; *Montes et al*., 2010]. North of 5°S, a near-surface coastal current flowing from Ecuador to Peru and associated with the surfacing of the EUC, has been suggested [*Lukas*, 1986; *Collins et al*., 2013]. This current is also partly resolved in mean near-surface circulation maps inferred from satellite-tracked drifters [*Albert et al*., 2010]. For clarity, and to avoid confusion with the eastward flowing EUC in subsurface, this poleward surface-trapped current will be referred to as the Ecuador-Peru Coastal Current (EPCC, Figure 1a). However, close to the Ecuadorian coast, a northwestward oriented surface current (the Coastal Ecuadorian Current, not shown in Figure 1a) can also take place [*Allauca*, 1990; *Collins et al*., 2013].

[3] Among the different currents that compose the NHCS, the PCUC is a key element because it advects seawater property anomalies from equatorial to extratropical regions and it plays a major role in the functioning of the NHCS ecosystem. The PCUC, that has been tracked along the continental shelf and upper slope from ~5°S off Peru to ~45°S off Chile [*Wooster and Gilmartin*, 1961; *Wooster and Reid*, 1963; *Silva and Neshyba*, 1979], carries a relatively warm, salty, nutrient-rich, oxygen-poor, and weakly stratified water mass of near-equatorial origin [*Silva and Neshyba*, 1979; *Tsuchiya and Talley*, 1998]. This water mass, the Equatorial Subsurface Water (ESSW), flowing southward into the PCUC is the main source of the coastal upwelled waters in NHCS promoting an intense primary productivity [*Brockmann et al*., 1980; *Huyer et al*., 1987; *Toggweiler et al*., 1991; *Chavez et al*., 2008; *Albert et al*., 2010]. Although the origin of the PCUC is still subject of scientific debate, it has been recognized that its main sources are the EUC and the two branches of the SSCC [*Montes et al*., 2010; *Czeschel et al*., 2011]. The general characteristics of the PCUC have been described from (i) the distribution of physical and biogeochemical water mass properties [*Gunther*, 1936], (ii) estimations of the circulation using the geostrophic approximation [*Wooster and Gilmartin*, 1961; *Wyrtki*, 1963; *Silva and Neshyba*, 1979], and (iii) direct measurements acquired from subsurface current meters [*Smith et al*., 1971; *Brink et al*., 1978, 1980; *Brockmann et al*., 1980; *Huyer et al*., 1991]. However, the majority of these studies were conducted more than three decades ago and existing data sets of direct subsurface current observations remain sparse. Recently, *Czeschel et al*. [2011] used shipboard acoustic Doppler current profiler (SADCP) data collected off Ecuador and Peru, but these data were acquired during a single cruise and the authors mainly focused on the mid-depth circulation of the NHCS. Between 2008 and 2012, the Peruvian Institute of the Sea (IMARPE) conducted 21 near-coastal cruises acquiring subsurface current measurements with an Ocean Surveyor SADCP. The main goal of this study is to analyze this extended database to provide a

Table 1. Names and Characteristics of the 21 Surveys Conducted Along the Peruvian Coast and Used in This Study: Initial and Final Dates, Latitudinal Coverage, and Number (N) of SADCP Profiles Retained for the Study

	Cruise	Start Date	End Date	Latitude Range (°S)	N
1	2008/02	7 Feb 2008	19 Feb 2008	10.02–6.63	245
2	2008/05-06	27 May 2008	26 Jun 2008	11.16–3.44	259
3	VOCALS REx 2008/10	3 Oct 2008	17 Oct 2008	18.30–12.15	334
4	2008/10-11	24 Oct 2008	1 Nov 2008	10.84–4.97	152
5	2008/11-12	23 Nov 2008	5 Dec 2008	12.38–7.18	221
6	2009/03-04	2 Mar 2009	13 Apr 2009	18.33–4.24	601
7	2009/06-07	12 Jun 2009	11 Jul 2009	12.03–3.42	411
8	2009/08-09	27 Aug 2009	27 Sep 2009	14.74–4.50	523
9	2009/10	21 Oct 2009	31 Oct 2009	18.19–12.56	220
10	2010/01-02	27 Jan 2010	17 Feb 2010	14.57–4.94	310
11	2010/02-04	27 Feb 2010	7 Apr 2010	18.33–4.96	501
12	2010/05-06	21 May 2010	14 Jun 2010	11.03–3.45	142
13	2010/08-09	21 Aug 2010	17 Sep 2010	13.33–4.50	447
14	2010/11-12	11 Nov 2010	22 Dec 2010	16.20–3.64	551
15	2011/02-04	26 Feb 2011	16 Apr 2011	18.30–3.41	719
16	2011/05-06	20 May 2011	18 Jun 2011	11.77–3.43	532
17	2011/08-10	31 Aug 2011	6 Oct 2011	15.48–4.99	643
18	2011/10	7 Oct 2011	12 Oct 2011	11.40–5.80	67
19	2011/10-12	31 Oct 2011	16 Dec 2011	17.87–3.58	610
20	2012/02-04	20 Feb 2012	13 Apr 2012	18.33–3.43	778
21	2012/05-06	2 May 2012	2 Jun 2012	11.96–3.43	470

comprehensive description of the circulation along the Peruvian coast, with a special focus on the mean PCUC dynamics and its spatio-temporal variability.

2. Data Sets and Methods

2.1. SADCP Data

[4] To assess the physical, biogeochemical, and biological conditions along the Peruvian coast for fishery resource assessment and follow up, IMARPE conducts multidisciplinary surveys from 4 to 5 times a year onboard its research vessels. Between February 2008 and June 2012, IMARPE's R/V *José Olaya Balandra* realized 21 such surveys, acquiring vertical profiles of horizontal currents (Table 1). These measurements were made using a RD Instruments Ocean Surveyor 75 kHz, hull-mounted SADCP. To avoid interference between the SADCP and a Simrad bifrequency EK60 echosounder, a synchronizer system was used. Raw SADCP data were acquired every 3 s, using a vertical bin length of 8 m with a 16 m blanking distance. The velocity estimates from each ping were vector-averaged into 10 min ensembles. The number of pings used in these 10 min mean values was ∼200 in average, and the depth range of good quality data (>30% good pings) was typically 16–600 m.

[5] The SADCP data were processed and calibrated using the Common Ocean Data Access System (CODAS) software developed at the University of Hawaii (E. Firing et al., University of Hawaii, unpublished manuscript, 1995). Data were required to pass tests of sufficient return signal, acceptable second derivatives of velocity components with respect to depth, and reasonable error velocities [*Zedel and Church*, 1987; Firing et al., unpublished manuscript, 1995]. The relative velocities were rotated from the transducer's to Earth's reference frame using the ship's gyrocompass. To determine absolute current velocities, navigation from the Global Positioning System (GPS) was used. A Blackman window of 30 min width was used to low-pass filter the reference layer (50–180 m) velocities. Errors on the orientation of the transducer relative to the gyroscopic compass and an amplitude correction factor for the SADCP were determined by standard calibration procedures [*Joyce*, 1989; *Pollard and Read*, 1989]. Typical amplitude errors of ∼1% and orientation errors of ∼1° were detected and corrected. Finally, in order to further filter out very high frequency variability and random residual noise, resulting calibrated velocity profiles were hourly averaged and vertically interpolated into 10 m bins from 25 to 705 m depth. SADCP profiles located over bathymetry shallower than 50 m depth were discarded.

[6] Figure 2a shows the spatial distribution of the 8736 hourly velocity profiles retained in this study. Velocity profiles are rather homogeneously distributed in latitude, although the amount of data slightly decreases south of ∼16°S. SADCP data were mainly recorded on the Peruvian shelf and continental slope with 50% of the profiles located above the 1000 m isobath (not shown). Data density drops offshore, with more than 75% (98%, respectively) of the velocity profiles distributed within 100 km (200 km) from shore. In the vertical, the number of data decreases from more than 8000 in the upper layers to less than 3000 below 500 m depth. Thus, due to the spatial distribution of the retained SADCP data, our analyses are mainly restricted horizontally from the coast to 200 km offshore and vertically from 25 to 500 m depth.

[7] The surveys were mostly conducted in February-June and September-November (Table 1) preventing the investigation of the near-coastal circulation variability at monthly scales. However, at seasonal scales (3 month periods), the number of data is rather homogeneously distributed (Figure 2), with a minimum of ∼1700 profiles in austral winter (July–September) and a maximum of ∼2400 profiles in austral summer (January–March) and fall (April–June). Therefore, in section 3.3, velocity profiles are

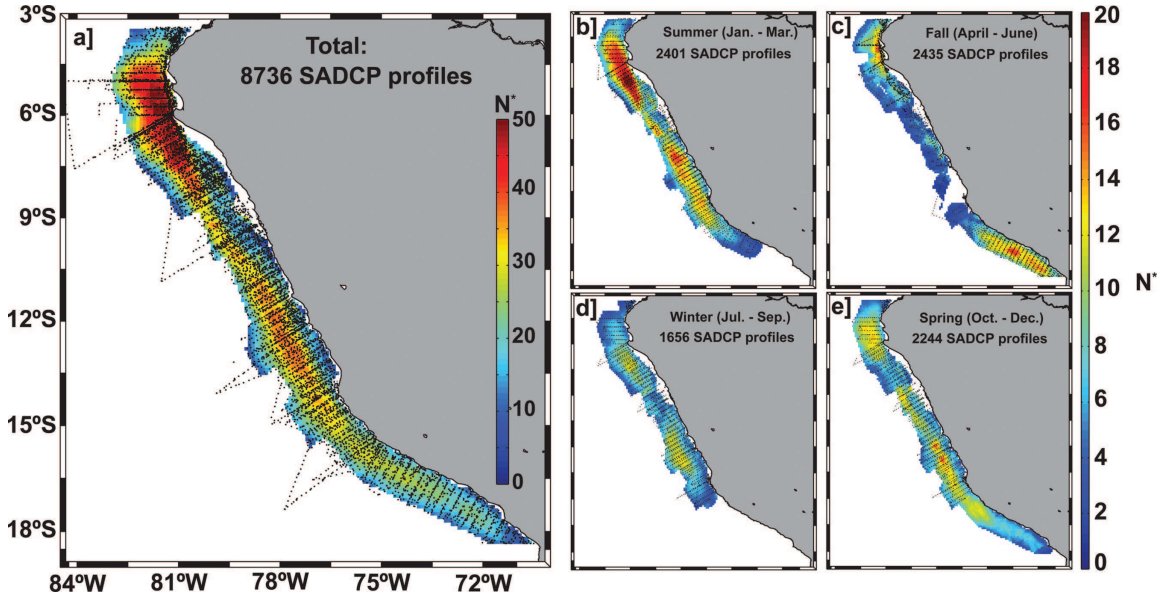

Figure 2. Spatio-temporal distribution of the 8736 hourly SADCP profiles retained in this study at (a) annual and (b–e) seasonal scales. The position of the SADCP profiles (black dots) overlaid on the number of depth-averaged independent observations (N^*, color shading) used to compute the mean circulation patterns (see text for details).

combined into 3 month periods to evaluate the seasonal variability of the alongshore circulation. Note, however, that the spatial distribution of the number of data is not homogeneous in time, with a smaller amount of observations between 12°S and 15°S in fall (Figure 2c) and South of ~16°S in summer and winter (Figures 2b–2d).

2.2. Gridding of SADCP Data

[8] The data were objectively analyzed on a 0.1° × 0.1° latitude-longitude grid depicted in Figure 2a (color shading). The methodology was adapted from *Hristova and Kessler* [2012]. First, at each grid point and at each 10 m vertical layer, velocity data located within 50 km from the grid point were selected. Second, an ellipse was defined with area of 157 km^2 (corresponding to an equivalent radius of 50 km) and axes oriented and scaled by the local velocity variance [*Johnson*, 2001; *Hristova and Kessler*, 2012]. SADCP profiles located inside this ellipse were selected and weight-averaged using an elliptical Gaussian weight function. The ellipses were mainly found to be elongated parallel to the coast, with a mean angle difference of 9° between the ellipse major axis direction and the coastline orientation. This preferred orientation allows improved representation of near-coastal currents. As mentioned by *Hristova and Kessler* [2012], the overlap of the bins means that each SADCP data contributes to the velocity estimate at several grid points, equivalent to spatial smoothing along the direction of maximum variance.

[9] At each grid cell, the error $\varepsilon_{\boldsymbol{U}}=(\varepsilon_U,\varepsilon_V)$ of the mean velocities $\boldsymbol{U} = (U,V)$ was evaluated using Student's t test with a significance level of 5%:

$$\varepsilon_{\boldsymbol{U}} = t_{N-1,0.025}\sqrt{\frac{\mathrm{var}\,(\boldsymbol{U})}{N^*}}$$

where $t_{N-1,0.025}$ represents the Student's t parameter, var$(\boldsymbol{U})$ is the velocity variance, and N^* the number of statistically independent observations. N^* was determined assuming that SADCP profiles separated by more than 50 km or 15 days are uncorrelated and independent. These decorrelation scales are larger than the typical Lagrangian time and length scales estimated in the eastern South Pacific from both near-surface drifters [*Zhurbas and Oh*, 2003; *Chaigneau and Pizarro*, 2005] and deep-sea mooring [*Klein*, 1993]. Using this method, we expect maximized error values, since the error variance is generally determined without multiplying it by Student's t parameter. Figure 2 shows the spatial distribution of the depth-averaged N^* computed from the whole SADCP data set as well as its seasonal variation.

[10] In section 3, we present averaged cross-shore or along-shore velocity sections $(\overline{U})$ and the corresponding transports. Averaged velocities and associated errors $(\varepsilon_{\overline{U}})$ are computed using a classical approach that consists to weight each velocity estimate by the inverse square of its error [e.g., *Roe*, 2001]:

$$\overline{U}\pm\varepsilon_{\overline{U}} = \frac{\sum \boldsymbol{U}/\varepsilon_{\boldsymbol{U}}^2}{\sum 1/\varepsilon_{\boldsymbol{U}}^2} \pm \sqrt{\frac{1}{\sum 1/\varepsilon_{\boldsymbol{U}}^2}}$$

[11] Transports ($\boldsymbol{T_U} = (T_U, T_V)$) and associated errors are computed through:

$$\boldsymbol{T}_{\boldsymbol{U}}\pm\varepsilon_{\boldsymbol{T}_{\boldsymbol{U}}} = \iint (\boldsymbol{U}\pm\varepsilon_{\boldsymbol{U}})dx\,dy.$$

[12] Note that diurnal and semidiurnal tidal amplitudes as well as near-inertial oscillations may cause aliasing in SADCP data. Unfortunately, we do not dispose of SADCP data at fixed stations occupied for several days that would allow us to document these oscillations using a classical

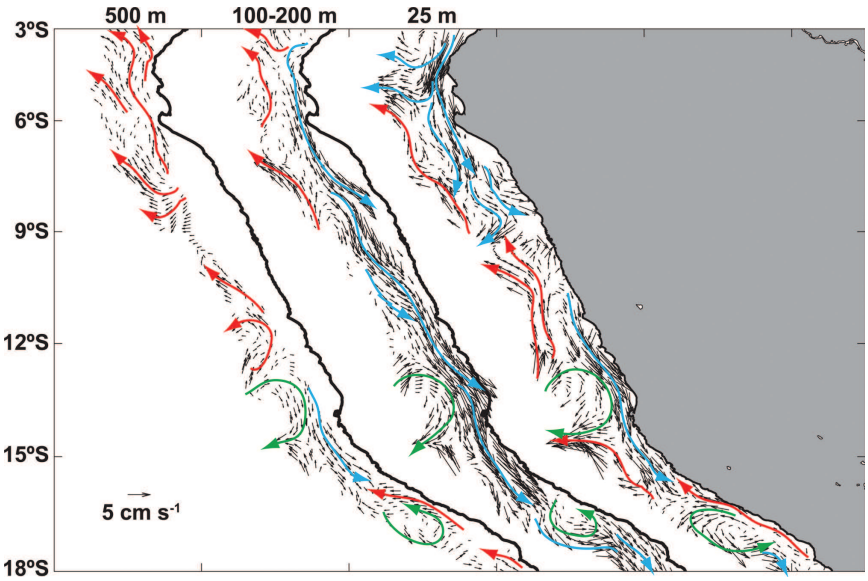

Figure 3. Mean current obtained from the interpolation of SADCP profiles at 25 m, between 100 m and 200 m, and 500 m depth. Red and blue arrows represent schematically the equatorward and poleward flows, respectively. Green arrows indicate the presence of mesoscale cyclonic (∼14°S) and anticyclonic (∼17°S) eddy-like features.

harmonic analysis. However, in the region under study, tidal current amplitudes are expected to be weak. For instance, in the shallow Coquimbo Bay (<50 m deep) located at 30°S where the tidal constituents show higher values than along the Peruvian coast [*Lyard et al*., 2006], tidal circulation estimated from ADCP data exhibit typical amplitudes of 10 cm s^{-1} [*Valle-Levinson et al*., 2000]. Between Pisco and Punta San-Juan (15°S–16°S), *Enfield* [1970] estimated semidiurnal amplitudes of 1–3 cm s^{-1} representing 10–15% of the mean speeds they measured. This author did not observe a significant spectral peak in the diurnal band frequency. Similarly, near-inertial currents along the Peruvian coast are among the weakest of the World Ocean [*Chaigneau et al*., 2008a]. From the global climatology of near-inertial current characteristics developed by *Chaigneau et al*. [2008] and distributed by the Centre de Topographie des Océans et de l'Hydrosphère (CTOH, Toulouse, France), the mean amplitude of the inertial currents in the energetic near-surface layer (0–15 m) along the Peruvian coast is 5–6 cm s^{-1}. In subsurface layers, *Enfield* [1970] did not observe significant inertial motions front of Pisco-San Juan.

[13] Thus, we believe that the mean circulation patterns presented in this study, obtained from the spatio-temporal filtering of numerous SADCP profiles recorded at different tidal and inertial phases, are not significantly affected by high-frequency motions. However, more caution needs to be taken with results based on individual cruises (section 3.4) that could be potentially impacted by high-frequency oscillations.

3. Results

3.1. Mean Near-Coastal Circulation

[14] The mean horizontal circulation and its schematic representation in a shallow (25 m), middle (averaged between 100 and 200 m), and deep layer (500 m) depth are presented in Figure 3. In the upper layer close to the coast, a relatively strong poleward flow (∼20 to 30 cm s^{-1}) is observed North of 5°S (Figure 3 at 25 m depth) associated with the EPCC. As mentioned in section 1, this current is probably related to the nearshore surfacing of the EUC that exhibits similar values near 3°S–4°S as it approaches the Ecuadorian and Peruvian coasts [*Collins et al*., 2013]. The EPCC, that originates from the EUC, mainly transports ESSW [e.g., *Lukas et al*., 1986; *Collins et al*., 2013]. However, being a near-surface current, the EPCC can also inject relatively warm and fresh (Figure 1) Equatorial Surface Water [*Strub et al*., 1998; *Fiedler and Talley*, 2006] along the Peruvian coast. At 5°S, the EPCC separates into two branches, one feeding the westward SEC and the other one continuing southward while weakening until ∼8°S– 9°S (Figure 3). A similar pattern was also recently observed in mean circulation maps computed from regional simulations at 60 m depth [*Albert et al*., 2010]. Between 8°S and 11°S–12°S the near-surface circulation is predominantly northward, associated with both the PCC and POC [*Wyrtki*, 1966; *Strub et al*., 1998] that transport relatively cold water from the south (e.g., Figure 1). Further south and particularly between 11°S and 16°S, a poleward flow of ∼10–15 cm s^{-1} is observed and is associated with the near-surfacing of the PCUC that is known to exhibit similar values in this region [*Huyer et al*., 1991; *Czeschel et al*., 2011]. South of 15°S, we also note the presence of a northward flowing current close to the coast, related to the PCC. Eddy-like mesoscale cyclonic and anticyclonic circulations are also observed, centered at ∼14°S and ∼17°S, respectively (green arrows in Figure 3 at 25 m depth). These mesoscale features, also observed in deeper layers (Figure 3), contribute to the trapping close to the coast and acceleration of the near-surfacing PCUC (12°S–14°S) and the PCC (16°S–17°S). These regions exhibit relatively high levels of

eddy kinetic energy and are known to be a preferential site of mesoscale eddy generation [*Chaigneau et al*., 2008b, 2009] which can have clear signatures in both the surface and subsurface layers [*Chaigneau et al*., 2011; *Colas et al*., 2012] and impact the characteristics of the large-scale circulation [e.g., *Czeschel et al*., 2011].

[15] In the middle layer (100–200 m depth), the circulation is clearly dominated by the presence of the poleward PCUC that extends all along the coast (Figure 3) and mainly transports ESSW in its core [*Silva and Neshyba*, 1979; *Tsuchiya and Talley*, 1998]. An intensification of the PCUC occurs between 8°S and 16°S, with mean values that can locally reach 20 cm s^{-1}. A recent modeling study, showed a similar intensification of the PCUC at 60 m depth [*Albert et al*., 2010]. North of 9°S and near the western boundary (∼200 km from the coast) of the domain under study, the mean circulation is also characterized by a northward/northwestward current, likely the POC, feeding the SEC. Between 16°S and 17°S, the offshoreward displacement of the PCUC is probably due to the presence of the mesoscale anticyclonic eddy-like feature.

[16] In the deep layer at 500 m depth, the average circulation is mainly northward, suggesting both a relatively deep vertical extent of the POC in the offshore ocean and the existence of a deep equatorward near-coastal current below the PCUC. This latter current was previously observed from in situ data [e.g., *Silva and Neshyba*, 1979; *Huyer et al*., 1987, 1991; *Strub et al*., 1998] and model simulations [*Penven et al*., 2005; *Montes et al*., 2011; *Colas et al*., 2012]. However, to the best of our knowledge, this deep northward current has not been specifically described except by *Czeschel et al*. [2011] who referred to it as the PCC [*Czeschel et al*., 2011, Figures 1 and 3]. Given that the deep current is clearly not related to the near-surface upwelling front forcing the PCC, we suggest, to avoid confusion, to refer to this current as the Chile-Peru Deep Coastal Current (CPDCC, see Figure 1b). This current that was also recently documented from high-resolution glider data, may transport relatively fresh and cold Antarctic Intermediate Water northward (A. Pietri et al., Impact of a coastal trapped wave on the near-coastal circulation of the Peru upwelling system from glider data, submitted to *Journal of Geophysical Research: Oceans*, 2013). Between 13°S and 16°S, a southward flow is still observed at 500 m (Figure 3) related to the deepening of the PCUC toward higher latitudes (see section 3.2). Although this deepening may be associated with the interaction between a cyclonic eddy and the PCUC, the SADCP data set is not sufficient to investigate the physical processes explaining this feature.

[17] As mentioned by *Penven et al*. [2005], the region located between 7°S and 13°S follows a quasi-rectilinear coastline and the bottom topography presents weak alongshore variations. In this area, the time-mean circulation should exhibit relatively homogeneous characteristics, except perhaps in the near-surface layers (Figure 3). Therefore, an alongshore average from 7°S and 13°S, which partly filters mesoscale structures, should be representative of the cross-shore structure of the central Peruvian upwelling circulation. Note that modeling studies usually depict the mean cross-shore properties of the Peruvian upwelling system, averaging hydrographic properties and currents in this latitude band [*Penven et al*., 2005; *Montes et al*., 2010, 2011; *Colas et al*., 2008, 2012]. Thus, Figure 4a aims to describe the mean alongshore circulation between 7°S and 13°S, and provides useful metrics for the validation of model simulations. The PCUC, corresponding to negative (mainly southeastward) alongshore velocity values, is clearly evidenced. Its core is centered in the upper part of the continental slope, with maximum averaged velocities higher than 10–11 cm s^{-1} at ∼100 m depth. The CPDCC flows equatorward below the PCUC, whereas the eastern flank of the equatorward POC is observed farther than 180 km from the coast. Standard errors associated with the mean alongshore velocity values and computed as described in section 2.2 are less than 0.5 cm s^{-1} in the major part of the section except within 40 km or farther than 190 km from the coast where they slightly increase to 0.8–1 cm s^{-1}. Note that the mean cross-shore section does not evidence the relatively thin and narrow PCC. The mean integrated transport in the 25–500 m layer (Figure 4b) is negative from the coast to 170 km offshore, with maximum negative values observed around 100 km above bathymetry of 300 m. The integrated alongshore transport between the coast and 200 km offshore is maximum in the core of the PCUC at 100 m depth and is poleward down to ∼320 m depth (Figure 4c). This depth approximately corresponds to the mean vertical extent of the PCUC in the central Peruvian upwelling region. The averaged total alongshore transport, integrated from the coast to 200 km offshore and from 25 to 500 m depth is of -1.6 ± 0.4 Sv.

3.2. Meridional Variations of the Near-Coastal Circulation

[18] The meridional variations of the near-coastal alongshore circulation are first illustrated by averaging cross-shore sections in five distinct latitudinal bands of 3° each (Figure 5). Between 3°S and 6°S, the continental slope is very steep and the southward alongshore flow is restricted to the upper 200 m, reaching velocity values higher than 12–13 cm s^{-1} in the near-surface layer at 25 km from the coast. This shallow current, also observed in Figure 3 and referred to as the EPCC, is associated with the surfacing of the EUC that can reach the south-American coast and typically extends over a similar 200 m surface layer [*Lukas*, 1986; *Collins et al*., 2013]. As mentioned previously, this current likely injects both ESSW from the EUC and Equatorial Surface Water along the Peruvian coast. The observed southward values are also consistent with surface-intensified velocities measured from current meters at ∼5°S [*Brockmann et al*., 1980] and from SADCP at ∼3.6°S [*Czeschel et al*., 2011]. In this northern region, the POC is seen farther than 100 km from the coast and the CPDCC below 300–400 m. The near-surface intensified equatorward current is also related to the northwestward deflection of the EPCC and the presence of a small-scale cyclonic recirculation cell at ∼3.5°S (see Figure 3). Similarly, the second core of southward flowing current observed at 150–200 km from the coast in subsurface (100 m depth), is associated with the small-scale anticyclonic recirculation cell observed at ∼5°S in the 100–200 m layer (see Figure 3) rather than with the PCCC observed at more than 200 km from the coast [*Czeschel et al*., 2011].

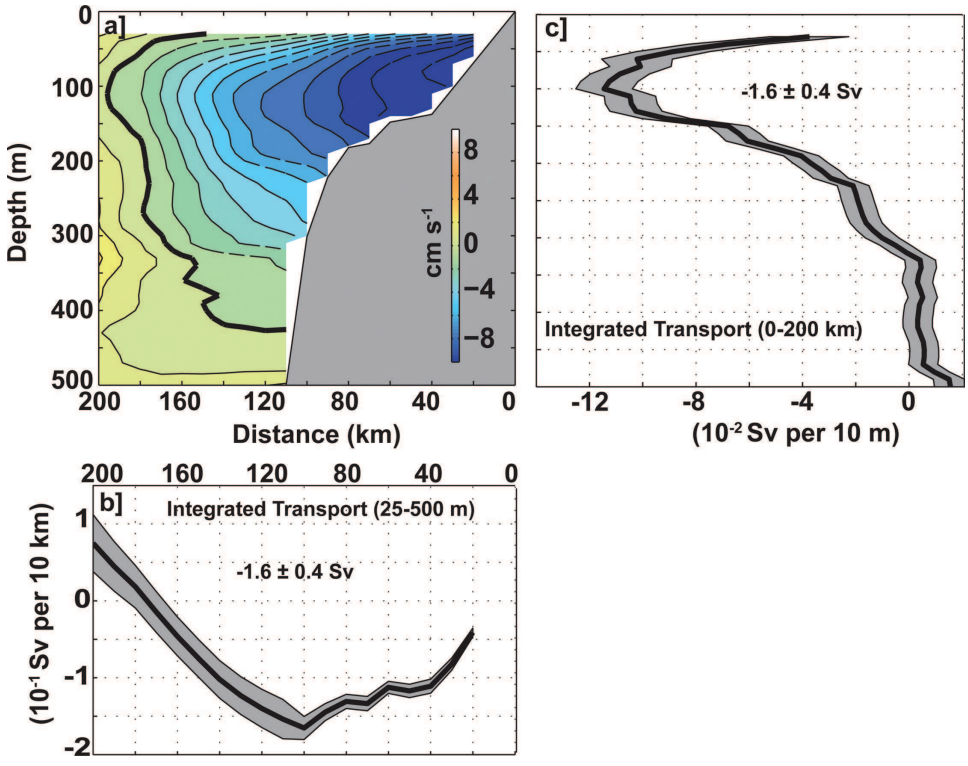

Figure 4. Mean cross-shore section (7°S–13°S) of the alongshore velocity component and integrated transports. (a) Mean cross-shore section of alongshore velocity (in cm s^{-1}) between the coast and 200 km offshore. (b) Mean cross-shore distribution of the alongshore transport integrated between 25 and 500 m depth. (c) Mean vertical profile of alongshore transport integrated from the coast to 200 km offshore. Gray shaded areas in Figures 4b and 4c represent errors around the mean (see text for details).

[19] Between 6°S and 9°S, where the continental shelf reaches its maximum width (∼110 km in average), the PCUC is centered inshore of the shelf break with maximum velocity values of ∼9 cm s^{-1}. The PCUC intensity is similar to the values of 6–8 cm s^{-1} obtained by *Penven et al*. [2005] in a regional numerical simulation off ∼6°S and ∼9°S. *Czeschel et al*. [2011] also observed a PCUC having a maximum southward velocity of 10 cm s^{-1} at 6°S in February 2009. In this region, the POC is located farther than 200 km from the coast (see also Figure 3) and the CPDCC is found below 300 m.

[20] Between 9°S and 12°S, the offshore extent of the continental shelf reduces in average to ∼70 km. The core of the PCUC is also centered inshore of the shelf break with maximum velocity values of 9 cm s^{-1} but extends offshore while deepening. Typical values of 10 cm s^{-1} were also observed in the core of the PCUC at 10°S from current meters [*Huyer et al*., 1991]. The PCC and POC are likely located farther than 90 and 180 km from the coast, respectively, whereas the CPDCC is found below 450 m depth.

[21] Between 12°S and 15°S, the continental shelf changes abruptly and the continental slope becomes steeper. The PCUC extends at least down to 500 m depth and its core is characterized by velocities higher than 14 cm s^{-1} that can be potentially enhanced by the presence of a cyclonic eddy (Figure 3). The observed mean values higher than 10 cm s^{-1} are consistent with previous measurements or estimations of the PCUC in this latitude band [*Brockmann et al*., 1980; *Brink et al*., 1980]. The POC is found farther than 160 km from the coast, whereas the CPDCC, probably flowing below the PCUC, is not sampled by the SADCP data set in this latitude band.

[22] Finally, between 15°S and 18°S, the continental slope gets even steeper and the PCUC occupies almost the

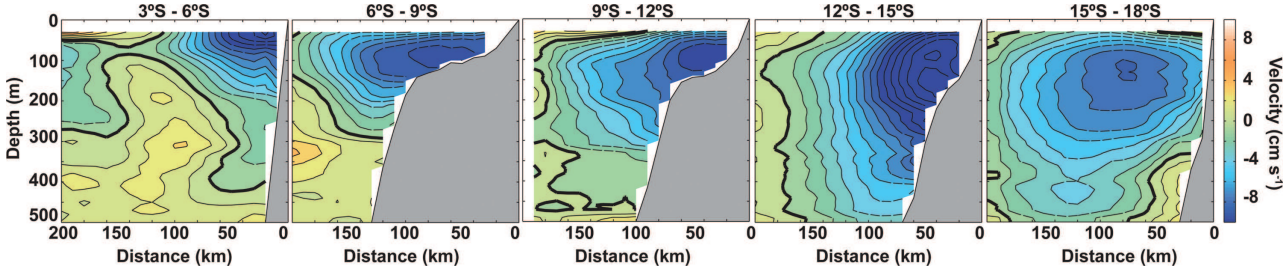

Figure 5. Mean cross-shore sections of the alongshore velocity (in cm s^{-1}) in different latitude bands.

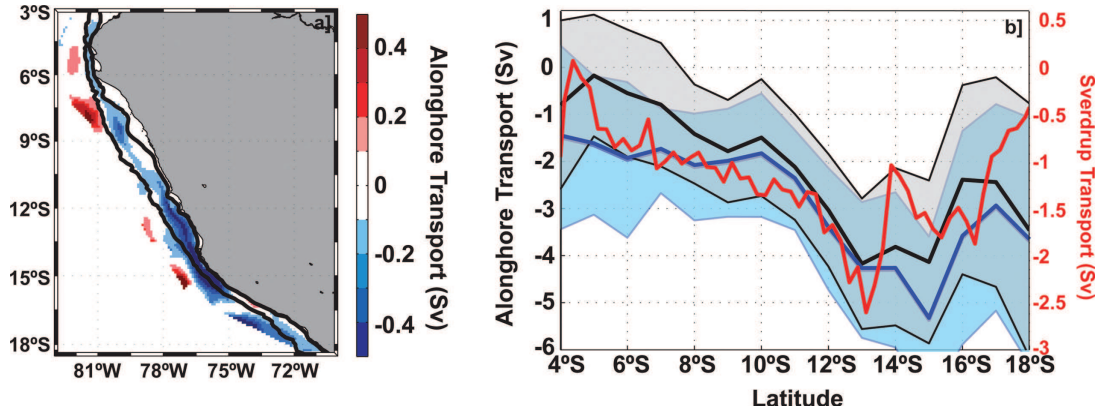

Figure 6. Alongshore transports (in Sv). (a) Alongshore transport integrated between 25 m and 500 m depth in 0.1° × 0.1° bins. Positive and negative transport values correspond to equatorward and poleward transports, respectively. Black solid lines corresponds to the 100 m and 2000 m isobaths. (b) Meridional variation in alongshore integrated transports (solid lines) and associated errors (shaded areas). Transports were integrated between 25 m and 500 m depth and from the coast to 200 km. Black solid line marks the total transport, whereas blue solid line corresponds to the transport associated with poleward alongshore velocity components only. Red solid line corresponds to the mean southward Sverdrup transport (2008–2012) integrated from the coast to 200 km offshore and computed from Metop/ASCAT winds.

entire cross section. In contrast with previous sections, the PCUC core with southward velocities higher than 7–8 cm s^{-1} is detached from the slope probably due to the presence of the anticyclonic eddy centered at ~16°–17°S (see also Figure 3). A part of the CPDCC is trapped on the slope below 300 m depth, whereas the main part is also probably flowing below the base of the PCUC beneath 500 m. Note that Figure 3 (500 m depth) shows a confluence between a poleward current and the CPDCC at 15°S, suggesting a deepening of the PCUC.

[23] The vertically integrated (25–500 m) alongshore transport across zonal bins of 0.1° reveals the presence of the southward flowing PCUC with typical values of 0.3 Sv that can reach 0.5 Sv locally between 12°S and 16°S (Figure 6a). As also observed in Figures 4 and 5, the PCUC is mainly trapped along the continental slope between isobaths of 100 and 2000 m (black solid lines in Figure 6a) except between 16°S and 17°S due to the anticyclonic structure. The estimated errors on these mean transport values are less than 0.2 Sv, except south of 15°S where the number of SADCP profiles slightly decreases and errors can locally increase to 0.3–0.4 Sv (not shown). Figure 6b shows the meridional variations of the integrated transport between the coast and 200 km offshore. South of 8°S, the total transport (black line in Figure 6b) is mostly dominated by the southward flow mainly associated with the PCUC (blue line in Figure 6b). In contrast, North of 8°S, the PCUC is counterbalanced by the northward flow observed both below it and offshore of the continental slope (Figures 5 and 6a), resulting in a slightly negative total alongshore transport (Figure 6b). The southward transport mainly associated with the PCUC (blue line in Figure 6b) is 1.8 Sv between 4°S and 10°S, and linearly increases southward to reach a maximum negative value of ~5.2 Sv at 15°S. South of 16°S, the PCUC transport is reduced, particularly at ~17°S, partly due to the anticyclonic eddy which disturbs the circulation and deflects the PCUC offshore (Figure 3). The transport value of ~1.8 Sv at 10°S is almost twice the transport estimated by *Huyer et al*. [1991] from hydrographic in situ data and geostrophic approximation at the same latitude. The averaged PCUC transport between 8°S and 13°S is of ~2.3 Sv, also much stronger than the 0.4–0.5 Sv estimated in the same latitude band from a regional model [*Echevin et al*., 2011].

[24] Figure 7a shows the meridional variation of the mean alongshore velocity averaged between the coast and 200 km offshore in each vertical layer. In the core of the PCUC, the mean southward alongshore velocity is 5–6 cm s^{-1}. Errors on the mean velocities are less than 1 cm s^{-1} except below 200 m depth between 7°S and 10°S and South of 16°S where errors can be higher than 2 cm s^{-1} (not shown). A particular feature observed in Figure 7a, that is further discussed in section 4.1, is the southward increase of the PCUC thickness. Below the PCUC, average positive velocities are a signature of both the POC that can extend vertically to at least 500 m depth and the CPDCC observed below the PCUC (Figures 3 and 5). Figure 7b shows the mean alongshore velocity between the coast and 200 km offshore taking only into account negative (poleward) components. North of 4°S, the poleward alongshore flow associated with the EPCC has a mean velocity reaching more than 15 cm s^{-1} that contrasts with the mean velocities associated with the PCUC further south. Part of the EPCC returns westward feeding the SEC (Figure 3), whereas the other part likely feeds the PCUC that is observed south of ~4°S–5°S with mean velocities reaching ~8 cm s^{-1} (see also Figure 5). The associated errors on these mean southward velocities are ±1 and 2 cm s^{-1} (not shown). The maximum southward velocities in each vertical layer and for all latitudes are presented in Figure 7c. The EPCC exhibits maximum velocities higher than 20 cm s^{-1}, whereas the PCUC core is characterized by maximum southward speeds varying between 10 and 15 cm s^{-1}.

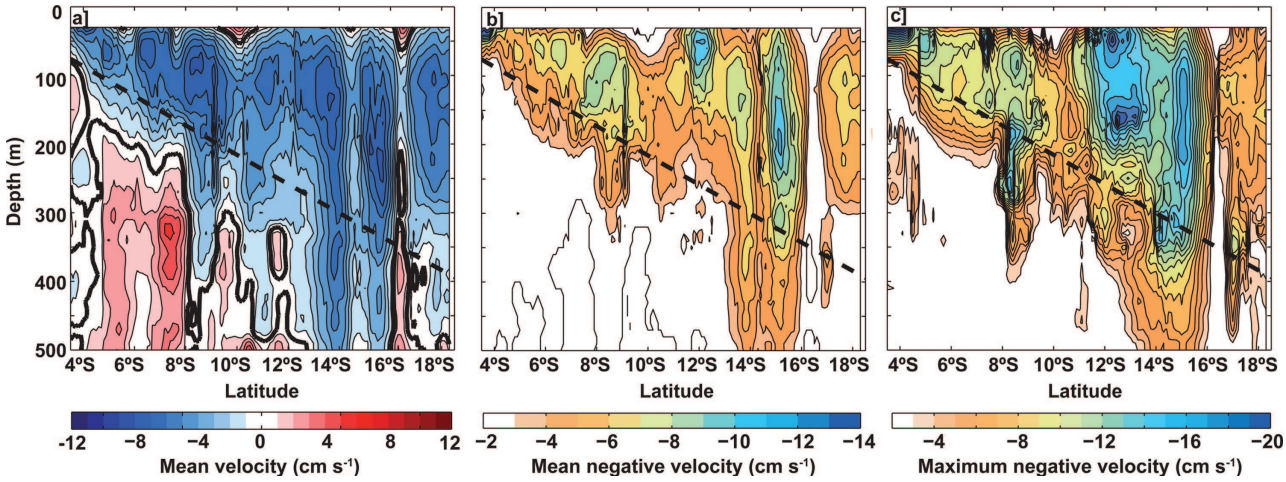

Figure 7. Alongshore section of time-mean alongshore velocities averaged between the coast and 200 km offshore (in cm s^{-1}). (a) Mean alongshore velocity, with black solid line separating the equatorward (positive values) alongshore flow from poleward alongshore flow (negative values). (b) Mean velocity considering only poleward alongshore flows. (c) Maximum poleward alongshore velocity. Black dashed lines in Figures 7a–7c represent the thickness (H) of the layer conserving its potential vorticity ($PV = fH = cst.$) from the value at 4°S.

3.3. Seasonal Variability of the Peru-Chile Undercurrent

[25] In order to provide some insights on the PCUC seasonal variability along the whole Peruvian coast from direct current observations, SADCP data were also sorted and gridded for four contrasted seasonal periods (summer: January-March; fall: April-June; winter: July-September; spring: October-December). Although the velocity profiles are quite homogeneously distributed among the four seasons (Figure 2), it is important to note that during summer (winter, respectively), almost 65% (70%) of the profiles were acquired in March (September).

[26] The alongshore circulation, averaged in a meridionally varying layer corresponding to the EPCC and PCUC cores, depicts interesting seasonal variations (Figure 8). The vertical extent of the EPCC and PCUC core layer is depicted in Figures 7–9 and its thickness varies from ~80 m at 4°S to ~400 m at 18°S. During summer, North of 4°S, the EPCC is relatively weak with mean southward velocity values of ~5 cm s^{-1} (Figure 8). At 5°S, this current is

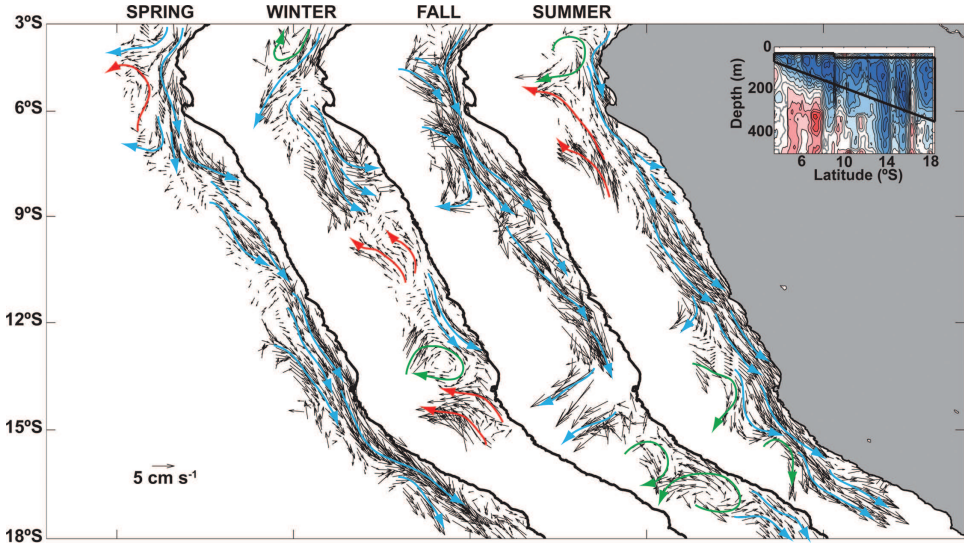

Figure 8. Seasonal cycle of the averaged circulation in the layer corresponding to the EPCC and PCUC core. Red and blue arrows represent schematically the equatorward and poleward flows, respectively, whereas green arrows indicate the presence of mesoscale eddy-like features. The vertical extent of the layer where the flow is averaged varies with latitude according to the black line depicted in the inset that corresponds to Figure 7a.

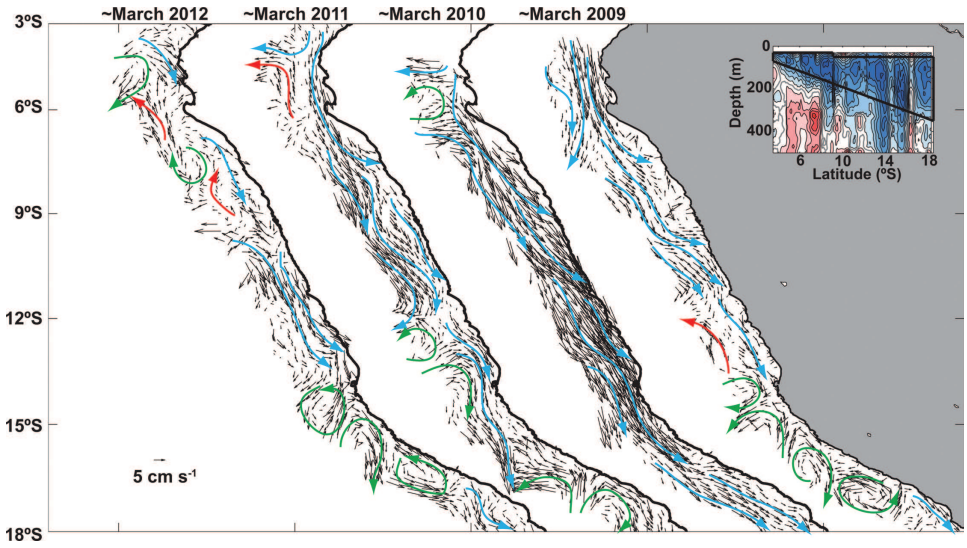

Figure 9. Same as Figure 8 but for specific March surveys realized along the Peruvian coast in 2009–2012.

found close to the coast and intensifies to 10–15 cm s^{-1}, probably due to the presence of an eddy-like cyclonic structure found slightly offshore. The PCUC is observed continuously along the coast and South of ~9°S, it intensifies and extends from the coast to 200 km offshore. Between 13°S and 16°S, the PCUC shows a meandering pattern, possibly associated with the presence of mesoscale eddies. Typical PCUC velocity values are of order of 10 cm s^{-1}, but they can locally reach more than 20 cm s^{-1}. During fall, the EPCC intensifies with mean velocity values of 10–15 cm s^{-1}. Further South, the PCUC shows similar velocity values that can locally reach 20–25 cm s^{-1}. The PCUC is likely fed by both the EPCC and an eastward flowing current entering the study domain near 5°S. This current could be related either to the southern branch of the EUC, reaching the Peruvian coast in this latitude range [e.g., *Lukas*, 1986], or to the pSSCC (Figure 1b) [see also *Czeschel et al.*, 2011]. Between 13°S and 15°S, the westward flow is probably not robust due to the small amount of independent data in this area. South of 15°S, we note the presence of an eddy dipole which disrupts the PCUC observed south of 17°S. In winter, the EPCC weakens and is of 5–10 cm s^{-1}, similar to the PCUC North of 9°S. During this season and South of 9°S, the PCUC pattern is unclear and disrupted by both northward intermittent currents and the presence of a cyclonic eddy at 13°S. In contrast during spring, the EPCC and PCUC are clearly observed along the whole Peruvian coast with velocities of 5–10 cm s^{-1}. South of 12°S, the velocity within the PCUC core increases to 15–20 cm^{-1}.

3.4. Interannual Variability of the Peru-Chile Undercurrent

[27] At interannual scales, El Niño Southern Oscillation (ENSO) events can strongly impact the near-coastal circulation of the NHCS. In particular, during strong El Niño (La Niña, respectively) events, the PCUC shoals (deepens) and intensifies (weakens) [*Huyer et al.*, 1991; *Colas et al.*, 2008; *Montes et al.*, 2011; *Dewitte et al.*, 2012]. In order to investigate part of the PCUC interannual variability, Figure 9 shows the circulation pattern in the PCUC core layer (the meridionally varying layer is the same as in Figure 8) for four specific surveys centered in March of four consecutive years (2009–2012, see Table 1). These cruises are the only ones covering the Peruvian region almost entirely.

[28] In March 2009, the EPCC-PCUC connection was relatively strong, with velocity values higher than 20 cm s^{-1} north of 6°S. South of 12°S, the circulation pattern was less clear and the presence of distinct mesoscale structures observed south of 14°S affected the PCUC flow. Some of these mesoscale features were also observed on satellite sea-level anomaly (SLA) maps (not shown). In March 2010, the EPCC was not adequately sampled but the PCUC was observed continuously from 6°S to 18°S. A strong intensification of the PCUC took place, with values higher than 30 cm s^{-1} between 9°S and 14°S. In March 2011, the EPCC was weaker than during March 2009 and a part of this current was deflected westward. Another part of the EPCC was trapped along the coast and fed the PCUC which was much weaker than during March 2010. Between 8°S and 12°S, the PCUC showed maximum values of 15–20 cm s^{-1} over the outer slope. South of 12°S mesoscale structures were again observed. Finally in March 2012, the circulation was much more complicated: the EPCC-PCUC connection was not seen, the PCUC was only observed between 10°S and 14°S, and distinct mesoscale eddies were sampled south of this latitudinal band. Thus, the most important feature observed in Figure 9 and further discussed in section 4.2 is the strong intensification of the PCUC observed in March 2010.

4. Discussion

4.1. Time-Mean Characteristics

[29] Based on the analysis of SADCP profiles acquired between 2008 and 2012 along the Peruvian coast, this study investigated the time-mean near-coastal circulation of the NHCS. Between the coast and 200 km offshore, this data set shows the presence of three main currents: (i) the POC,

only partly resolved by the SADCP data set, that flows equatorward in the offshore ocean, (ii) the PCUC that flows poleward along the continental shelf and slope, and (iii) the CPDCC that flows equatorward below the PCUC over the outer slope (Figures 4 and 5). Also, North of ~5°S, we have evidenced the presence of a relatively strong surface poleward current (Figures 3–5a) that is probably related to the near-surfacing of the EUC as it approaches the south-American coast along the equator [*Lukas*, 1986; *Collins et al*., 2013]. This current, referred to as the EPCC, has a mean velocity of 10–15 cm s^{-1} that can locally reach more that 20 cm s^{-1} (Figure 7). Using SADCP data from a single cruise realized between Ecuador and Galapagos Islands, *Collins et al*. [2013] documented the near-surfacing of the EUC near 3°S–4°S with values higher than 20 cm s^{-1} at 50 m depth. Similarly, *Lukas* [1986] estimated the geostrophic velocity of the EUC at 4°S to be of 30 cm s^{-1} at the surface. The continuity between the EPCC and the PCUC (Figures 7 and 8) suggests, in agreement with previous studies [*Wyrtki*, 1963; *Brink et al*., 1983; *Lukas*, 1986; *Toggweiler et al*., 1991; *Fiedler and Talley*, 2006], that the water transported by the PCUC would mainly originate from the EPCC and EUC. This contrasts with the recent modeling results of *Montes et al*. [2010] who showed that one of the main sources of the PCUC are the SSCCs. However, our data set does not extend sufficiently offshore in the near-equatorial region to allow clearly distinguishing between the eastward flowing SSCC and the EUC branch. Studies dealing with the merging of these subsurface currents with the near-coastal circulation of the NHCS, and the PCUC in particular, would thus require further dedicated survey experiments.

[30] The PCUC is on average centered over the outer continental shelf and inner slope at 100–200 m depth (Figures 4, 5, and 7) and typically transports ~2–3 Sv southward (Figure 6b). This southward transport increases progressively toward higher latitudes, particularly between 5°S and 15°S (Figure 6b). As mentioned by *Echevin et al*. [2011] and shown by *Albert et al*. [2010], the presence and intensity of the poleward undercurrent is strongly related to the local wind-stress curl through Sverdrup transport, as in other upwelling systems [e.g., *Marchesiello et al*., 2003]. The meridional variations of the integrated alongshore transport resemble those of the southward Sverdrup transport (red line in Figure 6b) induced by the nearshore negative wind-stress curl [*Albert et al*., 2010; *Risien and Chelton*, 2008]. However, this transport, estimated from monthly wind fields from advanced scatterometers (ASCAT/Metop) between 2008 and 2012 [*Bentamy and Croize-Fillon*, 2012] (ftp://ftp.ifremer.fr/ifremer/cersat/products/gridded/MWF/L3/ASCAT/) and integrated from the coast to 200 km offshore is about half the transport determined from SADCP data. There are several explanations for this discrepancy. First, scatterometer winds are inaccurate [*Croquette et al*., 2007] to study the dynamics close to the coast where a strong wind dropoff exists [*Capet et al*., 2004]. A better resolution of this wind dropoff would result in a stronger cyclonic wind-stress curl and associated southward Sverdrup transport. Second, the assumption of a negligible lateral friction in the Sverdrup relation may not be valid above the shelf and slope where strong frictional dissipation may take place. Third, the depth (500 m in our case) over which the transports are estimated does not correspond to the bottom of the ocean as assumed by the Sverdrup's theory. Fourth, the SADCP data set neither resolves the upper 25 m layer associated with a strong northward transport related to the PCC [*Albert et al*., 2010; *Echevin et al*., 2011], nor the deep ocean. This particularly concerns the full structure of the equatorward CPDCC that may decrease the total integrated alongshore transport estimated from SADCP data.

[31] Note that the southward transport increase is likely less associated with higher PCUC velocities (Figure 7a) than with an increase of the total area occupied by the PCUC, as depicted in Figure 7 by the deepening and increasing thickness of the PCUC toward higher latitudes. The deepening of the PCUC has been observed previously [e.g., *Silva and Neshyba*, 1979] and is probably explained by the conservation of potential vorticity (*PV*) [e.g., *Penven et al*., 2005]. Effectively, in the core of the PCUC, the Rossby number (R_0) can be estimated as:

$$R_0 = \frac{U}{fL}$$

where U and L are, respectively, characteristic velocity ($U \sim 0.1$ m s^{-1}) and length scales ($L \sim 10^5$ m) of the PCUC and f is the Coriolis parameter ($f \sim 1\text{–}5 \times 10^{-5}$ s^{-1}). Thus, the typical Rossby number is low ($R_0 = 2\text{–}8 \times 10^{-2}$); hence, the relative vorticity can be neglected in comparison with the planetary vorticity and the potential vorticity reduced to:

$$PV = f/H = cst.$$

where H is the thickness of the PCUC layer. At 5°S, the homogeneous PCUC layer is ~100 m deep (Figure 7a) and the corresponding *PV* is -1.3×10^{-7} s^{-1} m^{-1}. Conserving this *PV* value, the bottom part of the current should gradually increase southward as shown in Figure 7 (heavy dashed line). The observed deepening of the PCUC as it moves southward is in qualitative agreement with this linear relationship, suggesting that the PCUC thickness is partly a result of the conservation of potential vorticity. Note that this mechanism has been also recently proposed to explain the southward deepening of the undercurrent observed in the Benguela upwelling system [*Veitch et al*., 2010]. Other theoretical arguments can also be evoked to explain the poleward deepening and thickening of the PCUC. *Pizarro* [1999] reproduced its thickening along the Chilean coast between 20°S and 35°S using a wind-forced, continuously stratified, flat-bottom, linear model [*McCreary*, 1981]. Although this model is simplified in many aspects, it may also reproduce the observed PCUC deepening along the Peru coast.

[32] Along the Peruvian coast, SADCP data show that the PCUC core exhibits typical velocities of 5–10 cm s^{-1} with local intensification of ~20 cm s^{-1}, in agreement with previous works. From hydrographic cross-shore sections and considering the geostrophic approximation, the mean velocity inside the core of the PCUC off Peru was estimated to be of 5–10 cm s^{-1}, weakening in intensity to the south of 15°S [*Silva and Neshyba*, 1979]. From subsurface current meters anchored off 15°S over the continental slope off 15°S, velocity values acquired in 1969 and 1976 revealed a PCUC stronger than 20 cm s^{-1}. However, these two experiments took place during El Niño events, and the

observed high PCUC velocity values were suspected to be associated with these specific conditions [*Brockmann et al*., 1980]. In 1977, in the frame of the Estudio del Sistema de Afloramiento Costero en el Area Norte (ESACAN) and JOINT-II experiments, various current meters were deployed over the continental shelf and slope near 5°S, 10°S, 12°S, and 15°S [*Brockmann et al*., 1980]. Similarly, during the early 1980s, moored current meters registered velocity data over the inner continental margin off Peru. These data, acquired during periods associated with neutral environmental conditions, showed a maximum poleward flow of ∼10 cm s^{-1} at ∼100–150 m depth over the inner continental slope and outer shelf [*Brockmann et al*., 1980; *Brink et al*., 1980; *Huyer et al*., 1991]. More recently, using glider drift data collected in October-November 2008, *Pietri et al*. [2013] estimated the PCUC velocity to be of order of ∼15 cm s^{-1} at 15°S and at 200 m depth. The mean PCUC characteristics obtained in this study are also very consistent with the circulation depicted in regional modeling studies [*Penven et al*., 2005; *Montes et al*., 2010, 2011; *Echevin et al*., 2011; *Albert et al*., 2010].

[33] Local intensifications or weakening of the PCUC observed in Figures 5 and 7 can be explained by several mechanisms. Firstly, the large-scale currents described from SADCP data set are locally influenced by mesoscale activity, in particular, south of 15°S where the number of independent data decreases and eddy activity is relatively intense [*Chaigneau et al*., 2008b]. Mesoscale eddies could significantly modulate the PCUC through eddy advection or eddy mixing [*Montes et al*., 2010]. Using a single-cruise ADCP data set, *Czeschel et al*. [2011] also showed the presence of mesoscale eddies south of 15°S that locally disturb the signal associated with the large-scale circulation. Residual mesoscale circulation patterns can also be observed at various latitudes on the mean circulation computed from the average of seven years of model output [e.g., *Echevin et al*., 2011], suggesting that very long time series would be needed to filter out the transient mesoscale circulation in a climatology. Second, local changes of the shelf width, continental slope, or local bathymetry with the presence of small seamounts, islands or canyons may influence the undercurrent characteristics and intensity [e.g., *Huthnance*, 1984; *Zou and Holloway*, 1996; *Coelho et al*., 1999]. Third, local changes of the alongshore wind-stress and near-coastal cyclonic wind-stress curl can also impact on the PCUC characteristics [e.g., *McCreary*, 1981; *Mc Creary et al*., 1987]. Last but not least, alternating zonal jets observed from satellite altimetry [*Maximenko et al*., 2005; *Richards et al*., 2006; *Buckingham and Cornillon*, 2013], from Argo floats [*Cravatte et al*., 2012], and from model simulations [*Montes et al*., 2010] in the offshore ocean may also strongly interfere with the near-coastal subsurface circulation. Both a long-term monitoring of the near-coastal circulation with the acquisition of direct velocity observations and the implementation of process studies using high-resolution regional models are required to better interpret and understand the observed spatial variability of the PCUC characteristics.

4.2. Temporal Variability

[34] Due to its proximity to the equator, much of the variability of the Humboldt Current System is forced in the equatorial Pacific [*Huyer et al*., 1991; *Shaffer et al*., 1997; *Pizarro et al*., 2002; *Hormazabal et al*., 2002, 2006; *Ramos et al*., 2006]. At intraseasonal scales, wind-forced equatorial Kelvin waves generate free coastal-trapped waves (CTW) that propagate poleward along the south-American coast [e.g., *Clarke and Shi*, 1991; *Belmadani et al*., 2012]. CTW have a clear signature on sea level and modulate the PCUC with typical periods of 20–80 days [*Enfield*, 1987; *Huyer et al*., 1991; *Shaffer et al*., 1997; *Pizarro et al*., 2002; *Hormazabal et al*., 2002, 2006]. Off Peru at 10°S, *Huyer et al*. [1991] showed from current meter data that the dominant variability of the PCUC was in the 50 day band. In this study, the time-mean and seasonal circulation patterns were computed from numerous SADCP profiles recorded at different CTW phases and are thus likely representative of the mean states. In contrast, as discussed below, the PCUC characteristics depicted from individual cruises (e.g., Figure 9), might be strongly influenced by the equatorial wave dynamics and the passage of specific intraseasonal CTW.

[35] At seasonal scales, SADCP data along the Peruvian coast reveal that the observed PCUC is likely more intense in summer and fall and rather disorganized in winter (Figure 8). From previous studies based on both current meter data acquired at 10°S [*Huyer et al*., 1991] and regional model simulations [*Echevin et al*., 2011], only weak or inexistent seasonal variations are expected for the PCUC. *Echevin et al*. [2011] suggested that a weak PCUC intensification could take place during summer and fall, associated with the propagation of seasonal CTW forced by equatorial Kelvin waves. The weak PCUC intensification observed in the SADCP data set during these seasons (Figure 8) is not related to the seasonality of the nearshore wind-stress curl that is maximum in winter [*Echevin et al*., 2011, Figure 1]. Note that from hydrographic observations, *Lukas* [1986] also suggested an increase of the near-surfacing EUC transport during fall, coinciding with the maximum EPCC intensity shown in Figure 8. However, this author also mentioned that the near-surfacing EUC would exist only during this season, which strongly contrasts with the permanent EPCC observed between 3°S and 5°S (Figure 8). As mentioned by *Echevin et al*. [2011], the PCUC transport is driven by a complex combination of dynamical forcings such as the southward propagating coastal waves, the mesoscale activity, or the local wind-stress curl. Although the SADCP data set used in this study allowed a first assessment of the seasonal variability of the PCUC along the Peruvian coast, long-term observations would be needed to fully resolve and better understand the drivers of its seasonal cycle.

[36] At interannual scales, our data set revealed a strong intensification of the PCUC in March 2010 (Figure 9). In order to investigate the causes of such an intensification, two processes are proposed. First, the temporal variability of the alongshore-averaged Sverdrup transport anomaly does not show significant variations during the four surveys (black line in Figure 10a). This precludes the local wind forcing to be responsible of the PCUC intensification in March 2010. Second, one may wonder if this velocity increase is related to an ENSO event and associated equatorial wave dynamics. Following the national oceanic and atmospheric administration (NOAA) definition of El Nino events (http://www.cpc.ncep.noaa.gov/products/analysis_monitoring/ensostuff/ensoyears.shtml), a weak warm

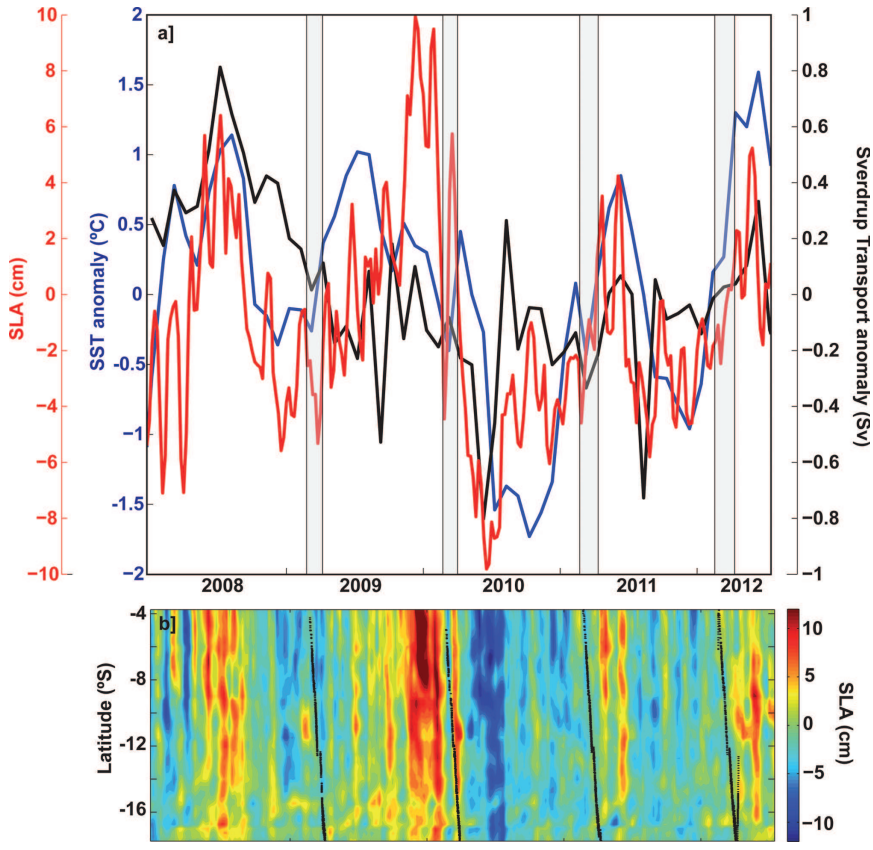

Figure 10. (a) Temporal variations of a coastal sea-level index (in cm, red line), SST anomalies in the Niño1+2 region (in °C, blue line) and Sverdrup transport anomaly (in Sv, black line). The sea-level index was obtained by averaging satellite sea-level anomalies (SLA) between the coast and 200 km offshore and between 3.5°S and 18°S. Sverdrup transport anomaly, relative to its seasonal cycle, was integrated from the coast to 200 km offshore and averaged between 3.5°S and 18°S. Gray shaded areas correspond to the timing of the four March surveys conducted in 2009–2012. (b) Hovmoller plot (time-latitude) of the SLA (in cm) averaged between the coast and 200 km offshore. Black dots represent the latitudinal position and time of the four surveys.

(El Niño-like) phase occurred from July 2009 to April 2010, while periods from November 2008 to March 2009, July 2010 to April 2011, and from September 2011 to March 2012 were considered as weak cold (La Niña-like) periods. A complete analysis of the ENSO cycle for 2008–2012 is beyond the scope of this paper, but data from the Tropical Ocean Atmosphere mooring array evidence that a series of downwelling Kelvin waves reached the eastern boundary of the Pacific between end 2009 and mid 2010 (not shown), coincidently with the strong PCUC of March 2010. Although during the four surveys, the sea-surface temperature anomalies in the Niño1+2 region were relatively weak and negative (−0.26°C in March 2009, −0.40°C in March 2010, −0.43°C in March 2011, and −0.27°C in March 2012, see blue line in Figure 10a), the equatorial Kelvin waves reached the south-American coasts and propagation of CTW along the Peruvian coast is evidenced in alongshore sea-level variations shown in Figure 10b. A particular feature is the passage of a wave train between October 2009 and March 2010 (Figure 10b). During this period, the alongshore-averaged SLA index (red line in Figure 10a) shows the passage of three downwelling CTW (i.e., associated with a positive nearshore SLA), one of which in March 2010 (SLA > 5cm) coinciding with the PCUC intensification (Figure 9). Note, however, that the cruise duration (∼1 month, see Table 1) is longer than the typical propagation time of a CTW along the Peruvian coast (e.g., Figure 10b). Although, the beginning of the cruise (from 5°S to 9°S), was associated with a weak negative SLA (Figure 10), the strongest intensification of the PCUC observed between 9°S and 14°S (Figure 9) effectively coincided with the passage of a downwelling CTW (Figure 10b). Therefore, the downwelling CTW following the equatorial Kelvin waves associated with the 2009–2010 weak El Niño event appears as a good candidate responsible of the observed PCUC intensification, as also suggested by regional modeling studies [*Colas et al.*, 2008; *Dewitte et al.*, 2012]. In contrast, the three other surveys, which did not take place during the passage of a similar CTW, did not show a notable PCUC increase. Note, however, that in March 2012, the circulation was relatively disorganized and the PCUC relatively weak (Figure 9). The causes of such a flow disorganization remains unexplained since (i) the alongshore-averaged Sverdrup transport does not show significant anomaly and (ii) no strong CTW propagated along the coast during this time period (Figure 10).

5. Concluding Remarks and Future Works

[37] This study, based on the analysis of a SADCP data set acquired by IMARPE between 2008 and 2012, provided a contemporaneous view of the near-coastal circulation in the NHCS. In particular, these data permitted to (i) investigate the PCUC characteristics at annual and seasonal scales along the Peruvian coasts, (ii) highlight the feeding of the PCUC by the EPCC North of 5°S, (iii) evidence the presence of the CPDCC flowing equatorward below the PCUC, and (iv) show the impact of a coastally trapped downwelling wave on the PCUC intensity. The obtained results provide an invaluable benchmark for evaluating the models used to study the regional circulation [e.g., *Penven et al*., 2005] and ecosystem [e.g., *Lett et al*., 2007; *Echevin et al*., 2008; *Albert et al*., 2010].

[38] There are remaining questions on the near-coastal dynamics in the NHCS that require further activities. First, although high-frequency variability associated with tides and near-inertial currents is relatively weak in the region [*Lyard et al*., 2006; *Chaigneau et al*., 2008a], the PCUC can exhibit relatively strong variations with periods of few days to few weeks [*Huyer et al*., 1991]. Also, recent studies based on the analysis of acoustic data revealed the presence of energetic variability at periods of few minutes/hours likely associated with internal waves [*Bertrand et al*., 2010; *Grados et al*., 2012]. These motions, which have a clear signature on the oxycline depth (∼20–100 m depth) and structure the ecosystem from macrozooplancton to forage fish, may also modulate the PCUC intensity. Thus, the implementation of continuous velocity measurements at fixed stations from SADCP or moorings would be needed to determine the high-frequency variability of the near-coastal circulation along the Peruvian coast. Furthermore, repetitive SADCP cross-shore sections occupied at nominal latitudes along the coast would allow to better determine the spatio-temporal variability of the PCUC at various scales.

[39] Second, the eastern South Pacific encompasses a large number of water masses that are continuously transported and mixed by the flows described in this study. For instance, the PCUC is known to mainly transport ESSW associated with high salinity and nutrients values and low dissolved oxygen concentrations [e.g., *Silva and Neshyba*, 1979; *Tsuchiya and Talley*, 1998; *Strub et al*., 1998]. However, the EPCC can also inject into the core of the PCUC (Figures 3, 7, 8, and 9) moderate salinity and nutrients-low Equatorial Surface Water found North of ∼4°S to 5°S in the near-surface layer (0–50 m) [e.g., *Lukas*, 1986; *Strub et al*., 1998; *Fiedler and Talley*, 2006; *Tsuchiya and Talley*, 1998]. Along the Peruvian coast, the PCUC can underlie both the upwelled Cold Coastal Water and the warmer and saltier Subtropical Surface Water found in the offshore ocean. South of ∼15°S to 20°S, the undercurrent can also move beneath a low salinity water known as the Eastern South Pacific Intermediate Water [e.g., *Schneider et al*., 2003; *Pietri et al*., 2013; Pietri et al., submitted manuscript, 2013]. Throughout the region under study, cold and low salinity Antarctic Intermediate Water lies beneath the PCUC [*Tsushiya and Talley*, 1998; *Fiedler and Talley*, 2006] and is partly transported northward by the CPDCC (Pietri et al., submitted manuscript, 2013). Thus, a blended analysis of the SADCP data with the IMARPE multidisciplinary physical (temperature, salinity) and biogeochemical (dissolved oxygen, nutrients, chlorophyll) data sets collected since the 1950s [e.g., *Gutiérrez et al*., 2011; J. Ledesma and C. Grados, 2012, personal communication] would probably help to determine the mean hydrological properties of the water masses transported by the distinct flows depicted in this study. In particular, the investigation of the progressive mixing of the ESSW with surrounding water masses during its southward advection by the PCUC would be important to better understand the role of this current on the connection between equatorial and extratropical regions.

[40] Third, the near-surface circulation of the upper 25 m surface layer could not be inferred from the current SADCP data set. However, since 2008, the number of satellite-tracked drifter deployments has been considerably increased along the Peruvian coast (C. Grados, personal communication). These data, together with newly developed satellite altimetry coastal products [e.g., *Durand et al*., 2008; *Le Hénaff et al*., 2010; *Roblou et al*., 2011; *Dussurget et al*., 2011] would help to study the spatio-temporal variability of near-surface currents associated with the PCC, POC, and EPCC. Finally, and as mentioned in section 4.1, a long-term sustained monitoring program in selected sites of the near-coastal region and the development of high-resolution coupled model platforms are required to further document the currents described in this manuscript and determine the respective role of the various forcings involved in the dynamics of the NHCS.

[41] **Acknowledgments.** We express our gratitude to the R/V *José Olaya Balandra* crew members and IMARPE oceanographers and supporting staff who recorded and made available SADCP data. Authors acknowledge the contribution of funding agencies. Most of the cruises were funded by the Peruvian government. The 2008/02 cruise (Filamentos) was cofunded by IMARPE and IRD. The coastal VAMOS Ocean-Cloud-Atmosphere-Land Study (VOCALS) Regional Experiment (REx) was cofunded by IMARPE, IRD, INSU, and the National Science Foundation. The altimetry data were produced by Ssalto/Duacs and distributed by AVISO, with support from CNES. The wind (SST, respectively) data are freely distributed by the IFREMER (NOAA). This manuscript, partly realized during stays of N. Dominguez at LEGOS and A. Chaigneau at IMARPE, is a contribution to the cooperation agreement for science research and technology signed between IMARPE and IRD and of the International Joint Laboratory—Dynamics of the Humboldt Current system (LMI—DISCOH). The authors particularly thank anonymous reviewers and Des Barton for their constructive comments that considerably helped to improve the manuscript. We are also grateful to F. Colas for fruitful discussions.

References

Albert, A., V. Echevin, M. Lévy, and O. Aumont (2010), Impact of nearshore wind stress curl on coastal circulation and primary productivity in the Peru upwelling system, *J. Geophys. Res.*, *115*, C12033, doi:10.1029/2010JC006569.

Allauca, S. (1990), Presencia de la corriente costanera ecuatoriana, *Acta Oceanogr. del Pacífico*, *6*(1), 10–17.

Belmadani, A., V. Echevin, B. Dewitte, and F. Colas (2012), Equatorially forced intraseasonal propagations along the Peru-Chile coast and their relation with the nearshore eddy activity in 1992–2000: A modeling study, *J. Geophys. Res.*, *117*, C04025, doi:10.1029/2011JC007848.

Bentamy, A., and D. Croize-Fillon (2012), Gridded surface wind fields from Metop/ASCAT measurements, *Int. J. Remote Sens.*, *33*(6), 1729–1754.

Bertrand, A., M. Ballón, and A. Chaigneau (2010), Acoustic observation of living organisms reveals the upper limit of the oxygen minimum zone, *PLoS ONE*, *5*(4), e10330, doi:10.1371/journal.pone.0010330.

Brink, K. H., J. S. Allen, and R. L. Smith (1978), A study of low frequency fluctuations near the Peru coast, *J. Phys. Oceanogr.*, *8*, 1025–1041.

Brink, K. H., D. Halpern, and R. L. Smith (1980), Circulation in the Peruvian upwelling system near 15°S, *J. Geophys. Res.*, *85*, 4036–4048, doi:10.1029/JC085iC07p04036.

Brink, K. H., D. Halpern, A. Huyer, and R. L. Smith (1983), The physical environment of the Peruvian upwelling system, *Prog. Oceanogr.*, *12*, 285–305.

Brockmann, C., E. Fahrbach, A. Huyer, and R. L. Smith (1980), The poleward undercurrent along the Peru coast: 5 to 15°S, *Deep Sea Res., Part A*, *27*, 847–856, doi:10.1016/0198-0149(80)90048-5.

Buckingham, C. E., and P. C. Cornillon (2013), The contribution of eddies to striations in absolute dynamic topography, *J. Geophys. Res. Oceans*, *118*, 448–461, doi:10.1029/2012JC008231.

Capet, X. J., P. Marchesiello, and J. C. McWilliams (2004), Upwelling response to coastal wind profiles, *Geophys. Res. Lett.*, *31*, L13311, doi:10.1029/2004GL020123.

Chaigneau, A., and O. Pizarro (2005), Mean surface circulation and mesoscale turbulent flow characteristics in the eastern South Pacific from satellite tracked drifters, *J. Geophys. Res.*, *110*, C05014, doi:10.1029/2004JC002628.

Chaigneau, A., O. Pizarro, and W. Rojas (2008a), Global climatology of near-inertial current characteristics from Lagrangian observations, *Geophys. Res. Lett.*, *35*, L13603, doi:10.1029/2008GL034060.

Chaigneau, A., A. Gizolme, and C. Grados (2008b), Mesoscale eddies off Peru in altimeter records: Identification algorithms and eddy spatiotemporal patterns, *Prog. Oceanogr.*, *79*, 106–119, doi:10.1016/j.pocean.2008.10.013.

Chaigneau, A., G. Eldin, and B. Dewitte (2009), Eddy activity in the four major upwelling systems from satellite altimetry (1992–2007), *Prog. Oceanogr.*, *83*, 117–123, doi:10.1016/j.pocean.2009.07.012.

Chaigneau, A., M. Le Texier, G. Eldin, C. Grados, and O. Pizarro (2011), Vertical structure of mesoscale eddies in the eastern South Pacific Ocean: A composite analysis from altimetry and Argo profiling floats, *J. Geophys. Res.*, *116*, C11025, doi:10.1029/2011JC007134.

Chavez, F., A. Bertrand, R. Guevara-Carrasco, P. Soler, and J. Csirke (2008), The northern Humboldt Current System: Brief history, present status and a view towards the future, *Prog. Oceanogr.*, *79*, 95–105, doi:10.1016/j.pocean.2008.10.012.

Clarke, A. J., and C. Shi (1991), Critical frequencies at ocean boundaries, *J. Geophys. Res.*, *96*, 10,731-10,738, doi:10.1029/91JC00933.

Coelho, H. S., R. R. Neves, P. C. Leitao, H. Martins, and A. P. Santos (1999), The slope current along the western European margin: A numerical investigation, *Bol. Inst. Esp. Oceanogr.*, *15*(1–4), 61–72.

Colas, F., X. Capet, J. C. McWilliams, and A. Shchepetkin (2008), 1997–1998 El Niño off Peru: A numerical study, *Prog. Oceanogr.*, *79*, 138–155.

Colas, F., J. C. McWilliams, X. Capet, and J. Kurian (2012), Heat balance and eddies in the Peru-Chile Current System, *Clim. Dyn.*, *39*(1-2), 509–529, doi:10.1007/s00382-011-1170-6.

Collins, C., A. Mascarenhas, and R. Martinez (2013), Structure of ocean circulation between the Galápagos Islands and Ecuador, *Adv. Geosci.*, *33*, 3–12, doi:10.5194/adgeo-33-3-2013.

Cravatte, S., W. S. Kessler, and F. Marin (2012), Intermediate zonal jets in the tropical Pacific Ocean observed by Argo floats, *J. Phys. Oceanogr.*, *42*, 1475–1485.

Croquette, M., G. Eldin, C. Grados, and M. Tamayo (2007), On differences in satellite wind products and their effects in estimating coastal upwelling processes in the south-east Pacific, *Geophys. Res. Lett.*, *34*, L11608, doi:10.1029/2006GL027538.

Czeschel, R., L. Stramma, F. U. Schwarzkopf, B. S. Giese, A. Funk, and J. Karstensen (2011), Middepth circulation of the eastern tropical South Pacific and its link to the oxygen minimum zone, *J. Geophys. Res.*, *116*, C01015, doi:10.1029/2010JC006565.

Dewitte, B., et al. (2012), Change in El Niño flavours over 1958–2008: Implications for the long-term trend of the upwelling off Peru, *Deep Sea Res., Part II*, *77–80*, 143–156.

Durand, F., D. Shankar, F. Birol, and S. S. C. Shenoi (2008), Estimating boundary currents from satellite altimetry: A case study for the east coast of India, *J. Oceanogr.*, *64*, 831–845.

Dussurget, R., F. Birol, R. Morrow, and P. De Mey (2011), Fine resolution altimetry data for a regional application in the Bay of Biscay, *Mar. Geod.*, *34*(3–4), 447–476.

Echevin, V., O. Aumont, J. Ledesma, and G. Flores (2008), The seasonal cycle of surface chlorophyll in the Peruvian upwelling system: A modelling study, *Prog. Oceanogr.*, *79*, 167–176.

Echevin, V., F. Colas, A. Chaigneau, and P. Penven (2011), Sensitivity of the Northern Humboldt Current System nearshore modeled circulation to initial and boundary conditions, *J. Geophys. Res.*, *116*, C07002, doi:10.1029/2010JC006684.

Enfield, D. B. (1970), A mesoscale study of coastal currents and upwelling off Peru, MS thesis, 67 pp., Oreg. State Univ., Corvallis.

Fiedler, P. C., and L. D. Talley (2006), Hydrography of the eastern tropical Pacific: A review, *Prog. Oceanogr.*, *69*(2–4), 143–180.

Grados, D., R. Fablet, M. Ballón, N. Bez, R. Castillo, A. Lezama-Ochoa, A. Bertrand, and D. Brickman (2012), Multiscale characterization of spatial relationships among oxycline depth, macrozooplankton, and forage fish off Peru using geostatistics, principal coordinates of neighbour matrices (PCNMs), and wavelets, *Can. J. Fish. Aquat. Sci.*, *69*(4), 740–754.

Gunther, E. R. (1936), A report on oceanographic investigations in the Peru Coastal Current, Discovery Rep. 13, pp. 107–276, Cambridge Univ. Press, Cambridge, U. K.

Gutiérrez, D., et al. (2011), Coastal cooling and increased productivity in the main upwelling zone off Peru since the mid-twentieth century, *Geophys. Res. Lett.*, *38*, L07603, doi:10.1029/2010GL046324.

Hormazabal, S., G. Shaffer, and O. Pizarro (2002), Tropical Pacific control of intraseasonal oscillations off Chile by way of oceanic and atmospheric pathways, *Geophys. Res. Lett.*, *29*(6), 1081, doi:10.1029/2001GL013481.

Hristova, H. G., and W. S. Kessler (2012), Surface circulation in the Solomon Sea derived from Lagrangian drifter observations, *J. Phys. Oceanogr.*, *42*, 448–458.

Huthnance, J. M. (1984), Slope currents and "JEBAR," *J. Phys. Oceanogr.*, *14*, 795–810.

Huyer, A., R. L. Smith, and T. Paluszkiewicz (1987), Coastal upwelling off Peru during normal and El Niño times, *J. Geophys. Res.*, *92*, 14,297–14,307, doi:10.1029/JC092iC13p14297.

Huyer, A., M. Knoll, T. Paluszkiewic, and R. L. Smith (1991), The Peru Undercurrent: A study of variability, *Deep Sea Res., Part A*, *38*, S247–S271.

Johnson, G. C. (2001), The Pacific Ocean subtropical cell surface limb, *Geophys. Res. Lett.*, *28*, 1771–1774.

Johnson, G. C., and D. W. Moore (1997), The Pacific subsurface countercurrents and an inertial model, *J. Phys. Oceanogr.*, *27*, 2448–2459, doi:10.1175/1520-0485(1997)027<2448:TPSCAA>2.0.CO;2.

Joyce, T. M. (1989), On the in-situ calibration of shipboard ADCP, *J. Atmos. Oceanic Technol.*, *6*, 169–172.

Karnauskas, K. B., R. Murtugudde, and A. J. Busalacchi, (2010), Observing the Galápagos–EUC interaction: Insights and challenges, *J. Phys. Oceanogr.*, *40*(12), 2768–2777.

Kessler, W. S. (2006), The circulation of the eastern tropical Pacific: A review, *Prog. Oceanogr.*, *69*(2–4), 181–217.

Klein, H. (1993), Near-bottom currents in the Deep Peru Basin, DISCOL experimental area, *Dt. Hydrogr. Z.*, *45*, 3142.

Le Hénaff, M., L. Roblou, and J. Bouffard (2010), Characterizing the Navidad current interannual variability using coastal altimetry, *Ocean Dyn.*, *61*, 425–437.

Lett, C., P. Penven, P. Ayon, and P. Freon (2007), Enrichment, concentration and retention processes in relation to anchovy (Engraulis ringens) eggs and larvae distributions in the northern Humboldt upwelling ecosystem, *J. Mar. Syst.*, *64*, 189–200.

Lukas, R. (1986), The termination of the equatorial undercurrent in the eastern Pacific, *Prog. Oceanogr.*, *16*, 63–90, doi:10.1016/0079–6611(86)90007-8.

Lyard, F., F. Lefevre, T. Letellier, and O. Francis (2006), Modelling the global ocean tides: Modern insights from FES2004, *Ocean Dyn.*, *56*, 394–415.

Marchesiello, P., J. C. McWilliams, and A. Shchepetkin (2003), Equilibrium structure and dynamics of the California Current System, *J. Phys. Oceanogr.*, *33*, 753–783, doi:10.1175/1520-0485(2003)33<753:ESADOT>2.0.CO;2.

Maximenko, N. A., B. Bang, and H. Sasaki (2005), Observational evidence of alternating zonal jets in the world ocean, *Geophys. Res. Lett.*, *32*, L12607, doi:10.1029/2005GL022728.

McCreary, J. P. (1981), A linear stratified ocean model of the coastal undercurrent, *Philos. Trans. R. Soc. London A*, *302*, 385–413.

McCreary, J. P., P. K. Kundu, and S.-Y. Chao (1987), On the dynamics of the California Current System, *J. Mar. Res.*, *45*, 1–32.

Mollier-Vogel, E., E. Ryabenko, P. Martinez, D. Wallace, M. A. Altabet, and R. Schneider (2012), Nitrogen isotope gradients off Peru and Ecuador related to upwelling, productivity, nutrient uptake and oxygen deficiency, *Deep Sea Res., Part I*, *70*, 14–25.

Montes, I., F. Colas, X. Capet, and W. Schneider (2010), On the pathways of the equatorial subsurface currents in the eastern equatorial Pacific and

their contributions to the Peru-Chile Undercurrent, *J. Geophys. Res.*, *115*, C09003, doi:10.1029/2009JC005710.

Montes, I., W. Schneider, F. Colas, B. Blanke, and V. Echevin (2011), Subsurface connections in the eastern tropical Pacific during La Niña 1999–2001 and El Niño 2002–2003, *J. Geophys. Res.*, *116*, C12022, doi:10.1029/2011JC007624.

Penven, P., V. Echevin, J. Pasapera, F. Colas, and J. Tam (2005), Average circulation, seasonal cycle, and mesoscale dynamics of the Peru Current System: A modeling approach, *J. Geophys. Res.*, *110*, C10021, doi:10.1029/2005JC002945.

Philander, S. G. H. (1973), Equatorial Undercurrent: Measurements and theories, *Rev. Geophys.*, *11*, 513–570, doi:10.1029/RG011i003p00513.

Pietri, A., P. Testor, V. Echevin, A. Chaigneau, L. Mortier, G. Eldin, and C. Grados (2013), Fine scale vertical structure of the upwelling system off Southern Peru as observed from glider data, *J. Phys. Oceanogr.*, *43*, 631–646, doi:10.1175/JPO-D-12–035.1.

Pizarro, O. (1999), Low frequency fluctuations in the eastern boundary current off South America: Remote and local forcing, PhD thesis, Göteborg Univ., Göteborg, Sweden.

Pizarro, O., G. Shaffer, B. Dewitte, and M. Ramos (2002), Dynamics of seasonal and interannual variability of the Peru-Chile Undercurrent, *Geophys. Res. Lett.*, *29*(12), 1581, doi:10.1029/2002GL014790.

Pollard, R., and J. Read (1989), A method for calibrating shipmounted acoustic Doppler profilers, and the limitations of gyro compasses, *J. Atmos. Oceanic Technol.*, *6*, 859–865.

Ramos, M., O. Pizarro, L. Bravo, and B. Dewitte (2006), Seasonal variability of the permanent thermocline off northern Chile, *Geophys. Res. Lett.*, *33*, L09608, doi:10.1029/2006GL025882.

Richards, K. J., N. A. Maximenko, F. O. Bryan, and H. Sasaki (2006), Zonal jets in the Pacific Ocean, *Geophys. Res. Lett.*, *33*, L03605, doi:10.1029/2005GL024645.

Ridgway, K. R., J. R. Dunn, and J. L. Wilkin (2002), Ocean interpolation by four-dimensional least squares—Application to the waters around Australia, *J. Atmos. Oceanic Technol.*, *19*(9), 1357–1375.

Risien, C. M., and D. B. Chelton (2008), A Global climatology of surface wind and wind stress fields from eight years of QuikSCAT scatterometer data, *J. Phys. Oceanogr.*, *38*, 2379–2413.

Roblou, L., J. Lamouroux, J. Bouffard, F. Lyard, M. Le Hénaff, A. Lombard, P. Marsalaix, P. De Mey, and F. Birol (2011), Post-processing altimiter data toward coastal applications and integration into coastal models, in *Coastal Altimetry*, edited by S. Vignudelli et al., chap. 9, 217–246, Springer, Berlin.

Roe, B. P. (2001), *Probability and Statistics in Experimental Physics*, 252 pp., Springer, New York.

Rowe, G. D., E. Firing, and G. C. Johnson (2000), Pacific equatorial subsurface countercurrent velocity, transport, and potential vorticity, *J. Phys. Oceanogr.*, *30*, 1172–1187, doi:10.1175/1520-0485(2000)030<1172:PESCVT>2.0.CO;2.

Schneider, W., R. Fuenzalida, E. Rodríguez-Rubio, J. Garcés-Vargas, and L. Bravo (2003), Characteristics and formation of eastern South Pacific Intermediate Water, *Geophys. Res. Lett.*, *30*(11), 1581, doi:10.1029/2003GL017086.

Shaffer, G., O. Pizarro, L. Djurfeldt, S. Salinas, and J. Ruttlant (1997), Circulation and low-frequency variability near the Chilean coast: Remotely forced fluctuations during the 1991–1992 El Niño, *J. Phys. Oceanogr.*, *27*, 217–235.

Silva, N., and S. Neshyba (1979), On the southernmost extension of the Peru-Chile Undercurrent, *Deep Sea Res., Part A*, *26*, 1387–1393, doi:10.1016/0198-0149(79)90006-2.

Smith, R. L., D. B. Enfield, T. S. Hopkins, and R. D. Pillsbury (1971), The circulation in an upwelling ecosystem: The Pisco cruise, *Invest. Pesq.*, *35*(1), 9–24.

Stramma, L., G. C. Johnson, E. Firing, and S. Schmidtko (2010), Eastern Pacific oxygen minimum zones: Supply paths and multidecadal changes, *J. Geophys. Res.*, *115*, C09011, doi:10.1029/2009JC005976.

Strub, P. T., J. M. Mesias, V. Montecino, J. Rutllant, and S. Salinas (1998), Coastal ocean circulation off western South America, in *The Sea*, vol. *11*, edited by A. R. Robinson and K. H. Brink, pp. 273–314, John Wiley, Hoboken, N. J.

Toggweiler, J. R., K. Dixon, and W. S. Broecker (1991), The Peru upwelling and the ventilation of the South Pacific thermocline, *J. Geophys. Res.*, *96*, 20,467–20,497, doi:10.1029/91JC02063.

Tsuchiya, M., and L. D. Talley (1998), A Pacific hydrographic section at 88°W: Water-property distribution, *J. Geophys. Res.*, *103*, 12,899–12,918.

Valle-Levinson, A., J. Moraga-Opazo, J. Olivares, and J. L. Blanco (2000), Tidal and residual circulation in a semi-arid bay: Coquimbo Bay, *Chile, Cont. Shelf Res.*, *20*, 2009–2028.

Veitch, J., P. Penven, and F. Shillington (2010), Modeling equilibrium dynamics of the Benguela Current System, *J. Phys. Oceanogr.*, *40*, 1942–1964.

Wooster, W., and M. Gilmartin (1961), The Perú-Chile Undercurrent, *J. Mar. Res.*, *19*, 97–122.

Wooster, W. S., and J. L. Reid (1963), Eastern boundary currents, in *The Sea: Ideas and Observations*, vol. *11*, edited by M. N. Hill, pp. 253–280, Wiley-Interscience, New York.

Wyrtki, K. (1963), The horizontal and vertical field of motion in the Peru Current, *Bull. Scripps Inst. Oceanogr.*, *8*, 313–344.

Wyrtki, K. (1966), Oceanography of the eastern equatorial Pacific Ocean, *Oceanogr. Mar. Biol. Annu. Rev.*, *4*, 33–68.

Wyrtki, K. (1967), Circulation and water masses in the eastern equatorial Pacific Ocean, *Int. J. Oceanol. Limnol.*, *1*, 117–147.

Zedel, L. J., and J. A. Church (1987), Real-time screening techniques for Doppler current profiler data, *J. Atmos. Oceanic Technol.*, *4*, 572–581.

Zhurbas, V., and I. S. Oh (2003), Lateral diffusivity and Lagrangian scales in the Pacific Ocean as derived from drifter data, *J. Geophys. Res.*, *108*(C5), 3141, doi:10.1029/2002JC001596.

Zou, J., and G. Holloway (1996), An effect of meso-scale bathymetry on eastern boundary undercurrent, *Dyn. Atmos. Oceans*, *25*, 133–142, doi:10.1016/0377-0265(95)00465-3.